Supporting Information for:

Photoacoustic Imaging of Human Mesenchymal Stem Cells Labeled with Prussian Blue-Poly(L-lysine) Nanocomplexes

Taeho Kim,[†] Jeanne E. Lemaster,[†] Fang Chen,[†, ‡] Jin Li,[†] and Jesse V. Jokerst[*, †, ‡, §]

[†]*Department of NanoEngineering*

[‡]*Materials Science Program*

[§]*Department of Radiology*

University of California, San Diego (UCSD), La Jolla, CA 92093.

Corresponding author: *jjokerst@ucsd.edu*

Supplementary Movie SM1. This video sequence is a real-time intraparenchymal injections of PB-labeled hMSCs (50×10^3) to a mouse brain. Left panel is B-mode (gray scale) and right panel is PA mode (red). White dashed circle indicates the injection site.

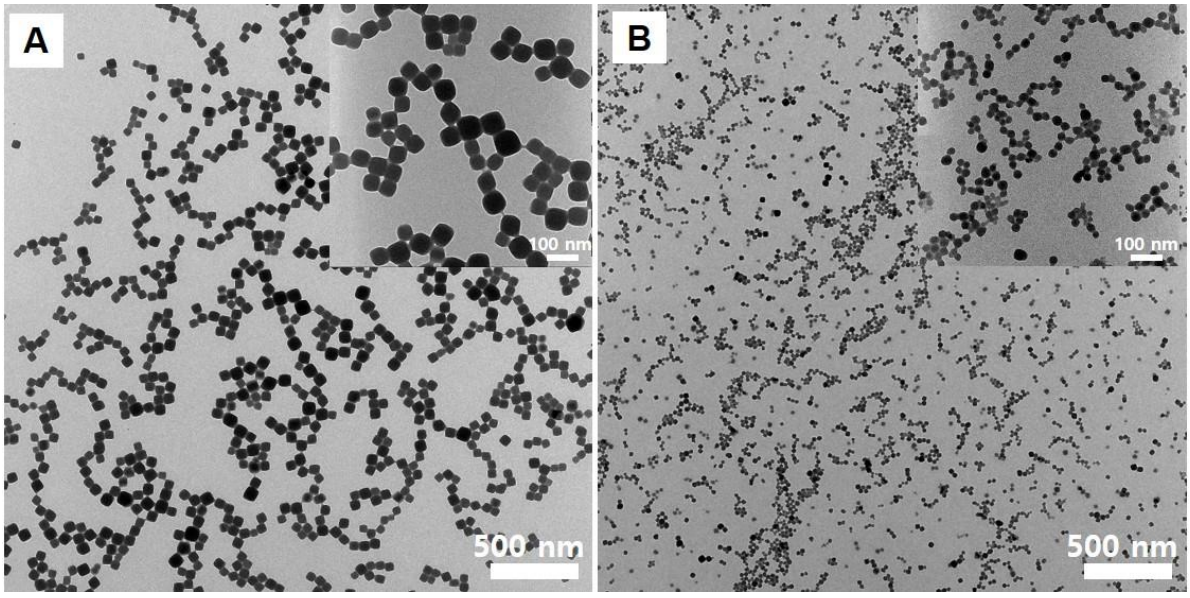

Figure S1. TEM of the prussian blue nanoparticles (PBNPs). (A) Lower-magnification and higher-magnification (inset) TEM images of prussian blue nanoparticles (PBNPs) of 50-60 nm. Scale bars are 500 nm and 100 nm, respectively. (B) Lower-magnification and higher-magnification (inset) TEM images of prussian blue nanoparticles (PBNPs) of 20-25 nm. Scale bar is 500 nm and 100 nm, respectively. Uniform and homogenous PBNPs capped in citric acid can be produced, and the size of PB NPs can be easily controlled by the amounts of citric acid. Smaller PBNPs (20-25nm) was synthesized when we used two-fold more citric acids. No difference in PA signal intensity was observed for the two different sizes of PBNPs.

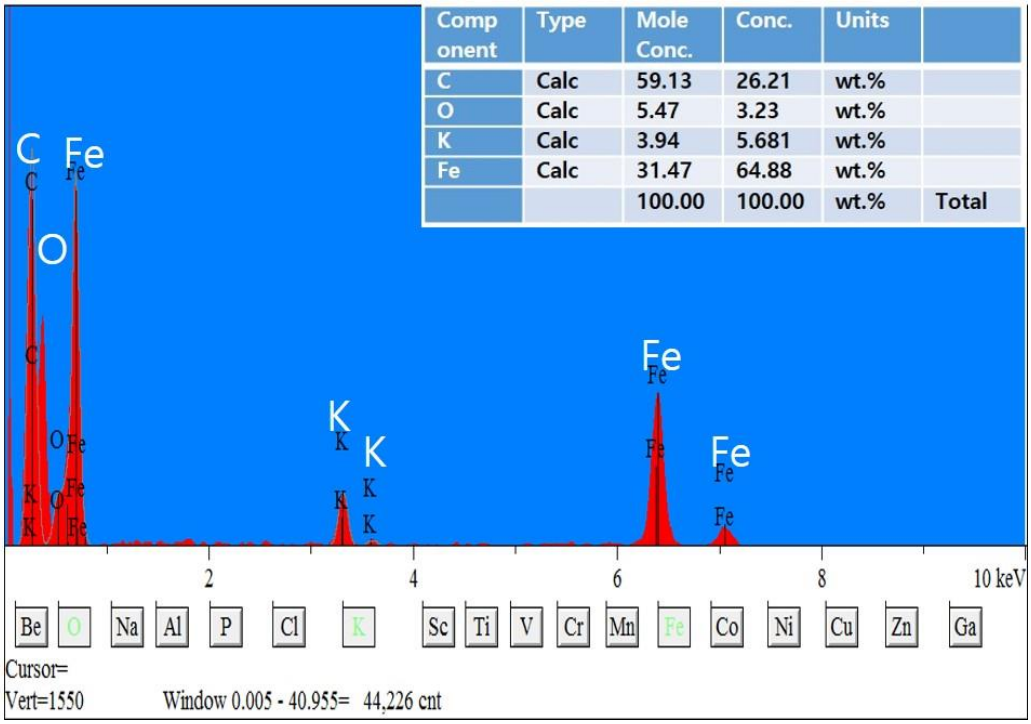

Figure S2. Energy-dispersed X-ray (EDX) spectrum. The data from PB NPs shows the presence of carbon, oxygen, potassium, and iron. The main element was iron (65%), and the approximate K:Fe ratio was 1:11.3, which indicates the most of as-prepared PBNPs are insoluble form of $Fe^{III}[Fe^{III}Fe^{II}(CN)_6]_3$.

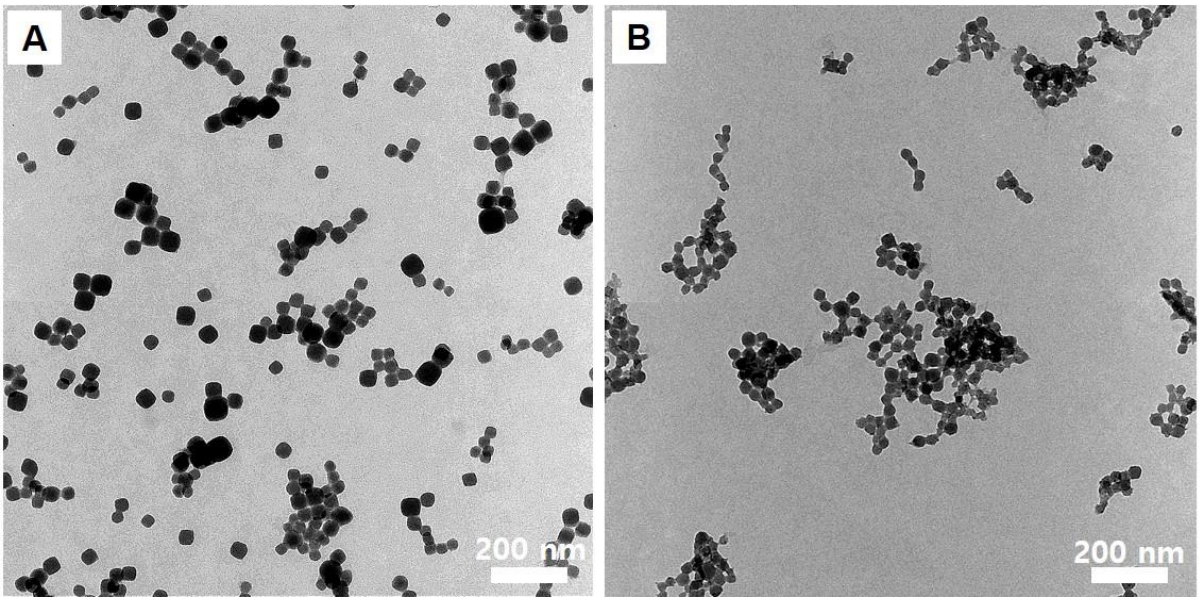

Figure S3. TEM of the PB-PLL nanocomplexes. (A) TEM images of PB-PLL nanocomplexes formed from 50-60 nm PBNPs. Scale bar is 200 nm. (B) TEM images of PB-PLL nanocomplexes formed from 20-25 nm PBNPs. Scale bar is 200 nm. Uniform and homogeneous PLL-coated PBNPs (PB-PLL nanocomplexes) were formed with larger PBNPs (50-60 nm), and their hydrodynamic diameter was 133.8 nm (PDI: 0.14) after complexation. However, smaller PBNPs (20-25 nm) had aggregations on complexation due to the insufficient coverages of PLL, and their hydrodynamic diameter increased to 225.3 (PDI: 0.44).

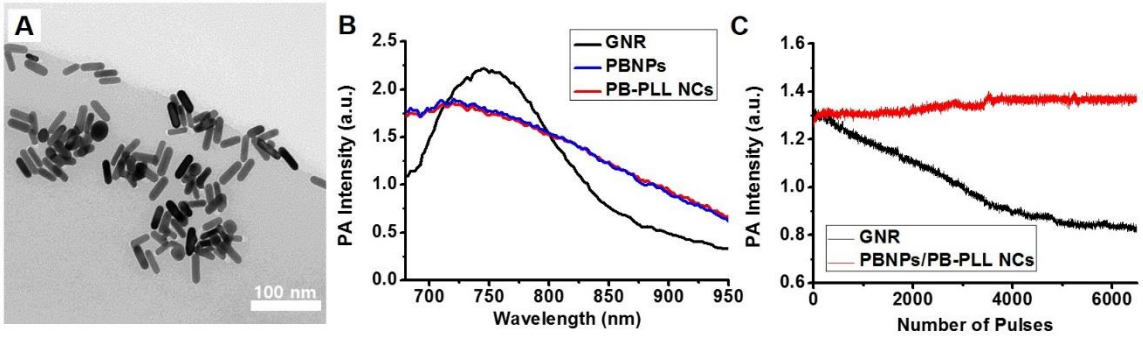

Figure S4. Comparison to gold nanorods. (A) TEM images of GNR. Uniform and discrete GNRs (15 × 50 nm) were synthesized. (B) Photoacoustic spectra of GNR (5 mg/mL), PBNPs (1 mg/mL), and PB-PLL nanocomplexes (1 mg/mL). GNRs have the highest photoacoustic signal at 750 nm. Both PBNPs and PB-PLL nanocomplexes show broad and intense signal between 650-900 nm and the highest photoacoustic signal at 730 nm, which corresponds to their absorbance spectra in Figure 1E. (C) Temporal stability of GNRs (5 mg/mL) and PBNPs (or PB-PLL nanocomplexes) (1 mg/mL). the signal of GNRs decreased by 38% after the exposure to 6.5×10^3 laser pulses (at 730 nm), the PBNPs (or PB-PLL nanocomplexes) were very stable.

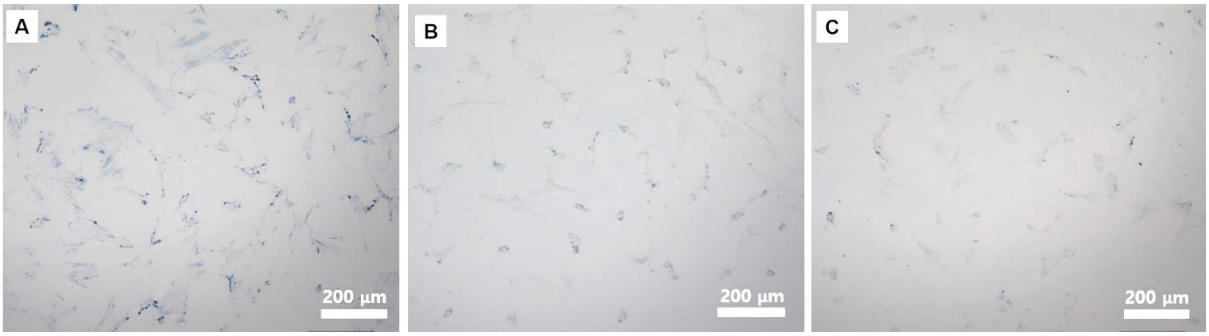

Figure S5. The mechanism of cellular uptake of PB-PLL nanocomplexes. (A) Bright field microscopy images of hMSCs incubated with PB-PLL nanocomplexes at 37 °C. Scale bar is 200 μm. (B) Bright field microscopy images of hMSCs incubated with PB-PLL nanocomplexes at 4 °C. Scale bar is 200 μm. (C) Bright field microscopy images of hMSCs co-treated with PB-PLL nanocomplexes and chemical inhibitor of endocytosis (dynasore; 10 μg/mL) at 37 °C. Scale bar is 200 μm. There was a significant decrease in cellular uptake on incubation at 4 °C or in the presence of endocytic inhibitors at 37°C—the bit depth of image (A) was 1.8-fold and 1.9-fold higher than that of image (B) & (C), and these findings suggest that PB-PLL nanocomplexes internalized to hMSCs by an energy-dependent uptake processes such as endocytosis.

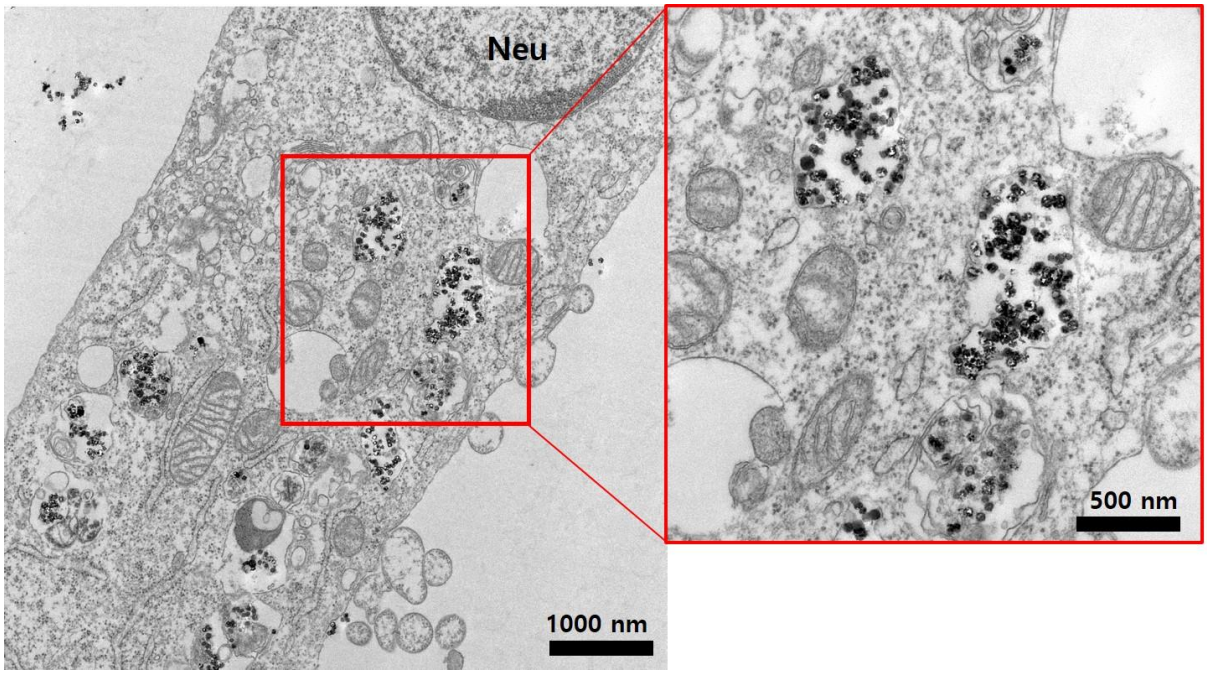

Figure S6. TEM images of labeled mouse mesenchymal stem cells (mMSCs). Similar to images from labeled hMSCs, PBNPs are dark and solid cubes. They showed a characteristic perinuclear, endosomal distribution. For cell TEM studies, 100 million mouse MSCs were incubated with PB-PLL nanocomplexs (50 μg/mL) for 6 hours. Neu indicates nucleus. Scale bars are 1000 nm and 500 nm, respectively.

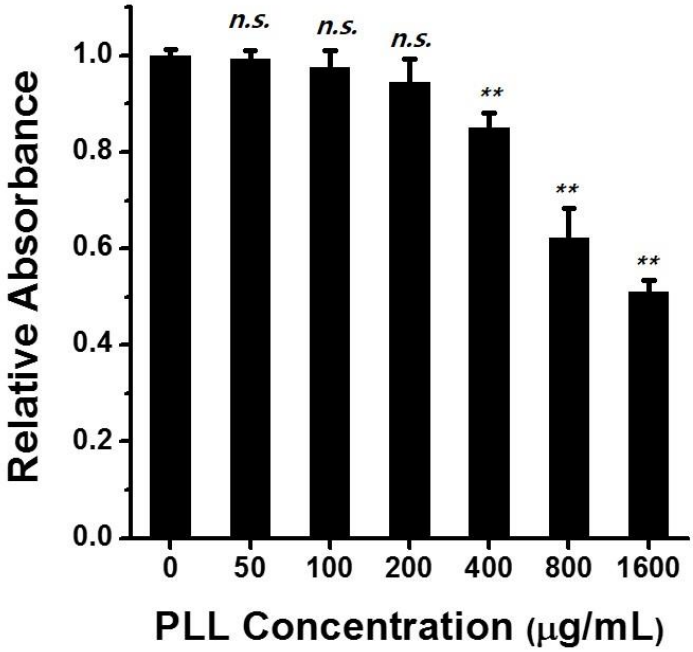

Figure S7. Assessment of cell viability using an MTS assay. hMSCs were incubated overnight with increasing PLL concentrations (0, 50, 100, 200, 400, 800, and 1600 µg/mL). PLL solutions are cytotoxic to hMSC at concentration over 400 µg/mL PLL. The statistical significance was calculated with the Student's t-test; **, $p < 0.01$; n.s., not significant *versus* the untreated control.

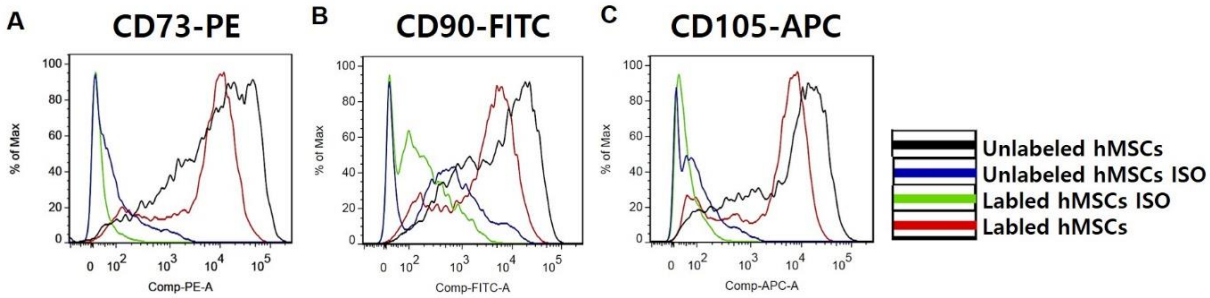

Figure S8. Flow cytometry data of MSC surface marker protein expression in unlabeled and labeled hMSCs. Similar to unlabeled hMSCs, the labeled hMSCs showed positive expression for surface markers of (A) CD73, (B), CD90, and (C) CD105. Whereas, isotype controls for unlabeled and labeled hMSCs had low signal.

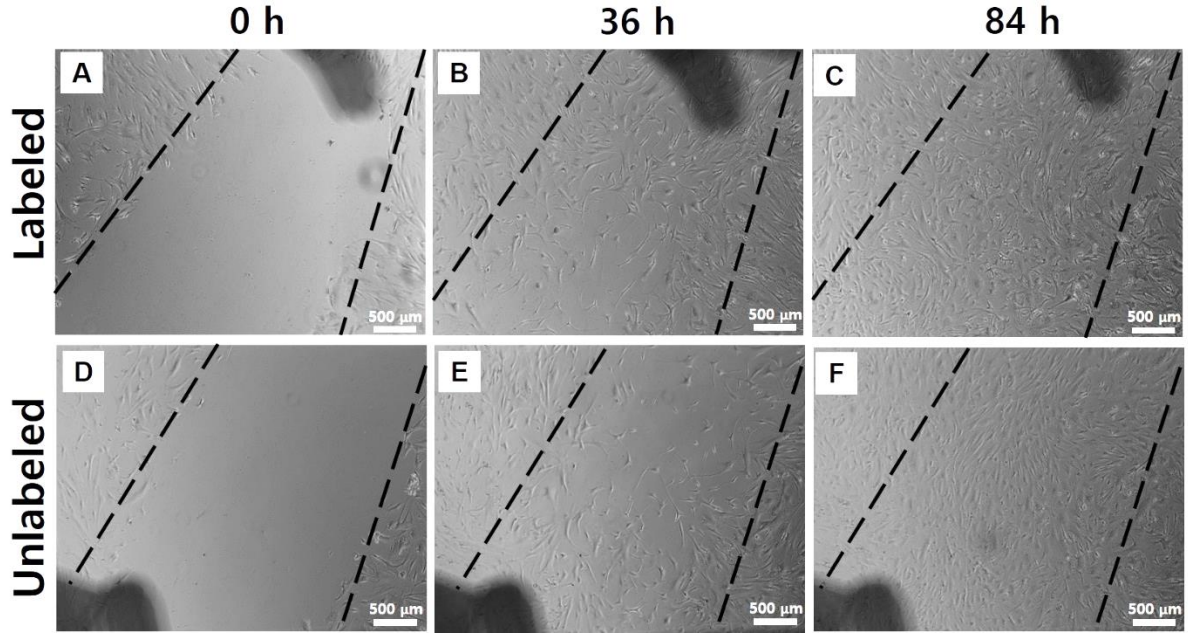

Figure S9. Cell migration assay. Migration capacity of hMSCs were studied by a Leica light microscopy with a monochrome camera at 0, 36, and 84 hours. Dashed lines was used to indicate the area where cells were removed, and the dark areas are fiducial markers to orient the plate for imaging. Both unlabeled (D, E, F) and PBNP-labeled hMSCs (A, B, C) successfully migrated to an area depleted of hMSCs within 36 hours. The scale bar is 500 µm.

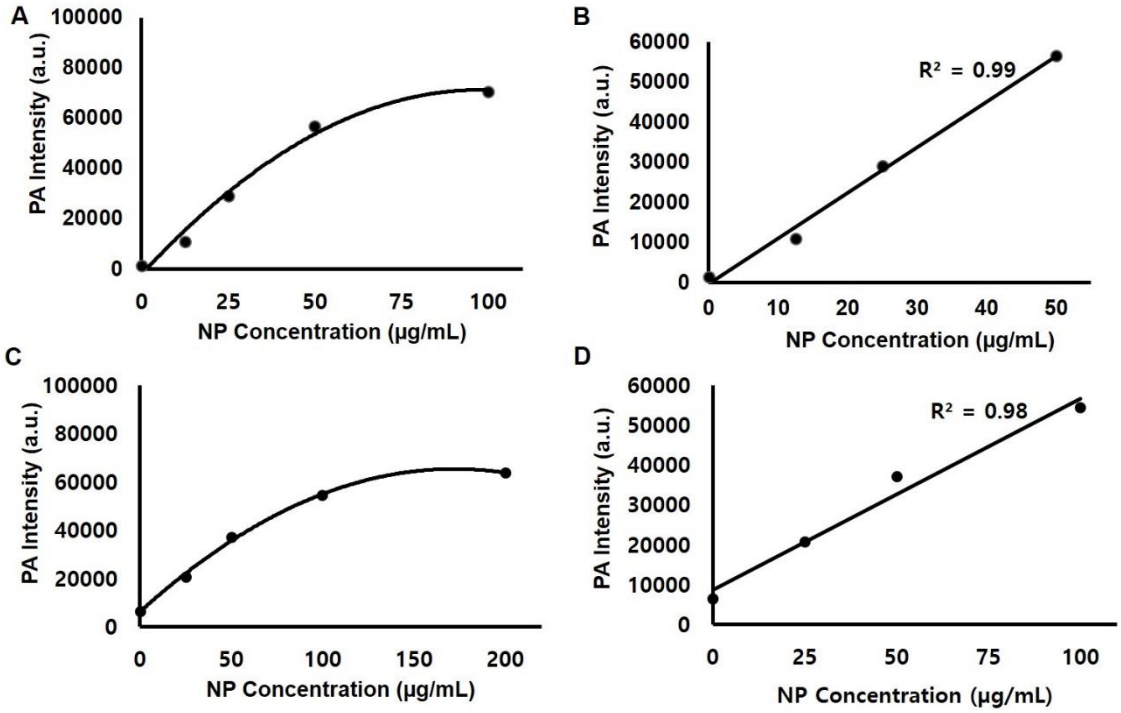

Figure S10. Labeling conditions. (A-B) PA images of 1% agarose suspension of 40 × 10^3 hMSCs (40% confluent in 6 well culture plate) with different concentrations of PB-PLL nanocomplexes (0, 12.5, 25, 50, and 100 μg/mL) and (C-D) 100 × 10^3 hMSCs (100% confluent in 6 well culture plate) with PB-PLL nanocomplexes (0, 25, 50, 100, and 200 μg/mL). The y-axis represents the PA intensity of 100 × 10^3 cells. (A-B) The PA intensity shows a linear relationship from 0-50 μg/mL (B); however there was a plateau at higher concentrations (50-100 μg/mL) (A). We repeated this with fully confluent cells and again saw that the PA intensity linearly increased at lower concentrations but plateaued above 100 μg/mL. This indicates that the cells simply cannot internalize any more nanoparticles and defines the upper limit of the incubation concentration (C-D).

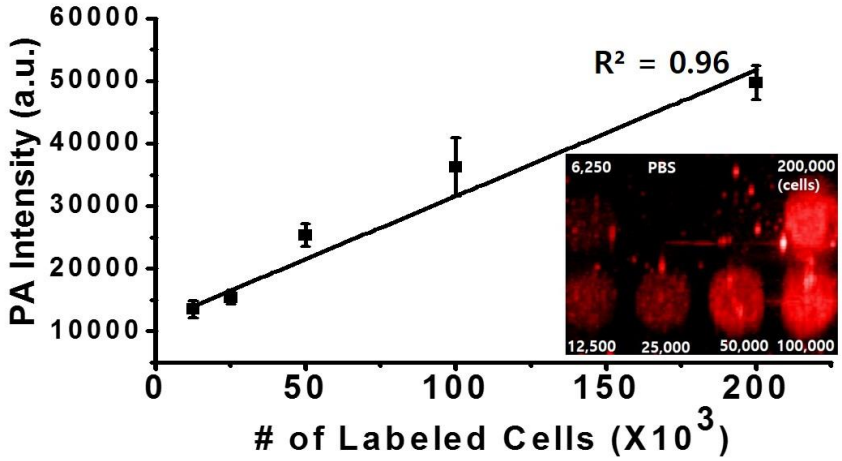

Figure S11. Linear plot of photoacoustic signal intensity *versus* # of labeled hMSCs. Here, 5×10^3 – 200×10^3 cells were imaged *in vitro*. The inset shows the corresponding photoacoustic images for the plot. Error bars represent the standard deviation.

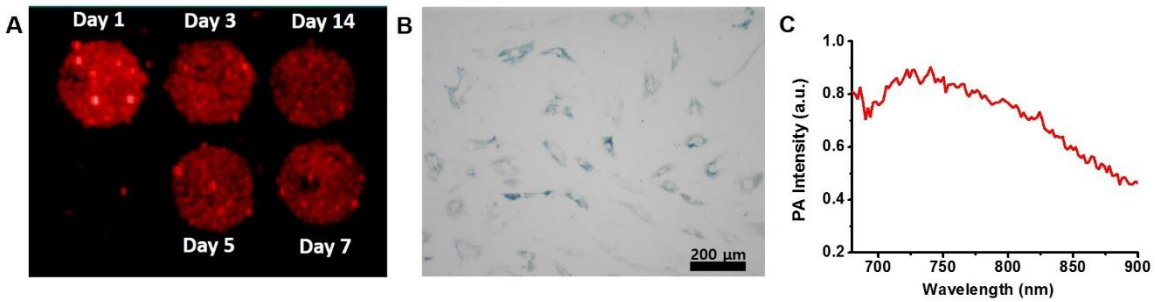

Figure S12. The longitudinal photoacoustic data for labeled hMSCs *in vitro*. (A) There was sustained PA signal over 2 weeks of culture. (B) The PB nanoparticles remained labeled even after 2 weeks of expansion in the culture plate. (C) Spectral photoacoustic signal of labeled cells shows broad and intense light signal from 650-950 nm similar to samples of PBNPs only.

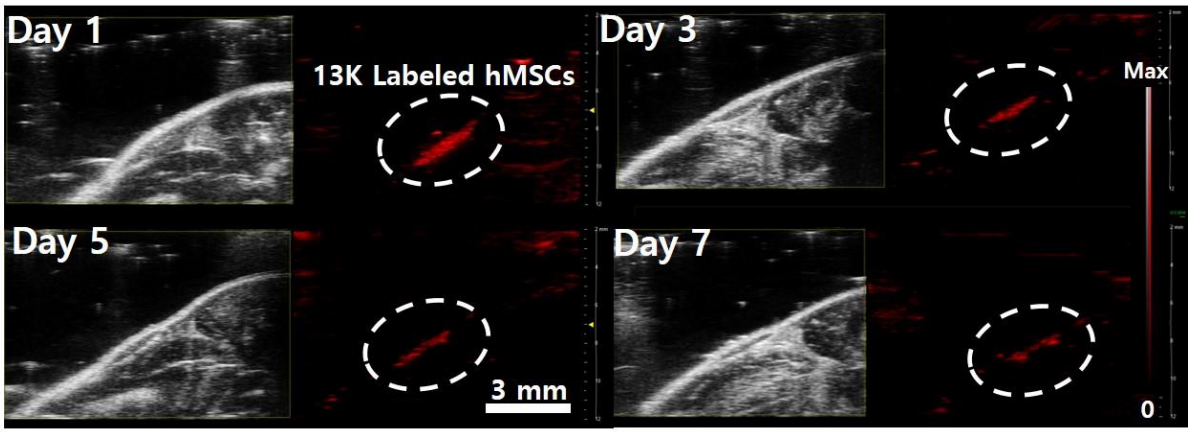

Figure S13. The longitudinal PA imaging of transplanted cells *in vivo*. Here, 13×10^3 hMSCs were subcutaneously injected into nude mice. An intense PA contrast was detected upon transplantation (day 1), however their contrast decreased upon serial PA imaging, which made it difficult to discern them from the background signals on day 7.

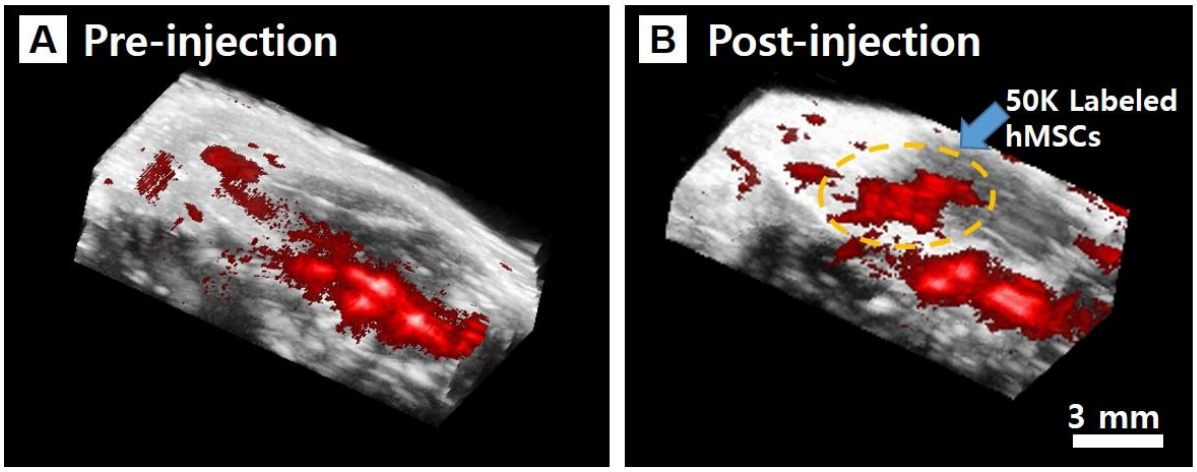

Figure S14. 3D reconstruction of PA images of a nude mouse brain after transplantation of 50 × 10^3 labeled cells. US/PA combined images before injection (A) and after injections (B). Yellow dashed circle indicates the injection site of labeled cells (50 × 10^3 hMSCs).

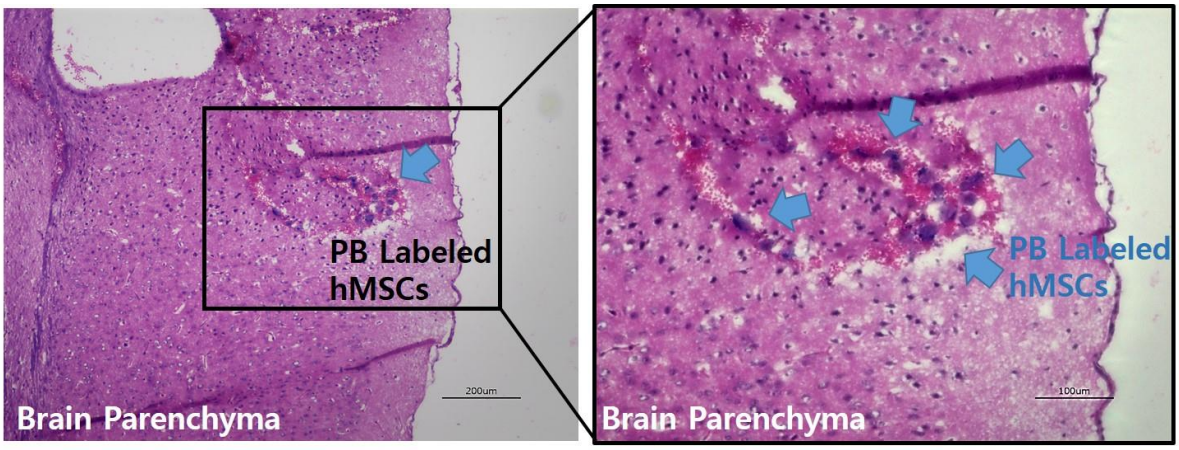

FigureS15. H&E Staining of brain tissue with injected cells. PBNP-labeled hMSCs was seen in blue color (indicated by blue arrows) and detected in the injected locations on the surrounded brain tissue.